Renewable Energy 147 (2020) 437–446

Contents lists available at ScienceDirect

Renewable Energy

journal homepage: www.elsevier.com/locate/renene

Trailing-edge serrations effect on the performance of a wind turbine

Elena Llorente [a, *], Daniele Ragni [b]

[a] Nordex Energy Spain S.A.U, Avenida Ciudad de la Innovacion, 3, 31621, Sarriguren, Navarra, Spain
[b] Aerodynamics, Wind Energy, Flight Performance and Propulsion Department, Faculty of Aerospace Engineering, Delft University of Technology, Kluyverweg 1, 2629, HS Delft, the Netherlands

ARTICLE INFO

Article history:
Received 31 January 2019
Received in revised form
5 August 2019
Accepted 26 August 2019
Available online 28 August 2019

Keywords:
Trailing-edge serrations
Flap angle
Wind tunnel tests
Aerodynamic coefficients
Wind turbine loads
Wind turbine power curve

ABSTRACT

An experimental study focusing on the change of the aerodynamic performance of a wind turbine with the employment of trailing-edge serrations is presented. The design procedure which starts from the serration design, together with the experimental wind tunnel testing and the installation in an already operating wind turbine is discussed. A prediction methodology to estimate the aerodynamic performance change of the machine with the blade add-on is validated by in-field measurements. Wind tunnel experiments for the validation of the original serration design have been carried out on a Nordex ADO30 airfoil with a relative thickness of 30% and on a NACA64$_3$418 airfoil with 18% thickness. The two airfoils are respectively used in this study due to their peculiar characteristics. While the first has been designed for relatively high Cl/Cd performance versus structural integrity (i.e. relatively high thickness), the second one is a typical reference airfoil used in wind turbines for its interesting Cl/Cd performance in both laminar and rough conditions. Clean and rough conditions have been tested in order to prepare a database for the analysis of the full turbine in several wind conditions. Aerodynamic forces with the serrated trailing-edge extensions are measured for different angles of attack and serration flap angles. The results are further discussed and employed for the analysis of the full rotor. Results already show that an increase in the flap angle is typically associated with an increment in lift, but not necessarily in drag. This has a beneficial effect on the operational regime of the machine when taken into account. The influence of the trailing-edge serrations on an operating wind turbine has been quantified in terms of total loads and energy production. The power curves with and without the trailing-edge installations are further analyzed and compared with the theoretical predictions.

1. Introduction

The use of trailing-edge serrations for mitigating the airfoil self-noise emitted by wind turbine blades has become very popular in the wind energy industry. Its efficacy in reducing the most important aeroacoustic component originated by the interaction of the airfoil turbulent boundary-layer with the blade trailing-edge has been proven in many studies, theoretically [1,2], numerically [3] and experimentally [4–6]. While the physical principle behind the noise reduction was already elucidated by Howe's work [1], predicting the magnitude of the noise reduction and its frequency range is not an easy task. The main effect of the serrated edge is to effectively reduce the spanwise length of the trailing-edge that contributes to noise generation [1]. Since the first study from Howe, a large number of experimental studies on trailing-edge serrations have focused on applications such as 2D airfoils and wind turbine blades. Amongst many, Jones et al. [3] performed DNS simulations over the NACA-0012 airfoil with a flat-plate trailing-edge with and without serrations, to investigate the link between flow structures, aerodynamic performance and noise reduction capabilities. Gruber et al. [5] in their experimental work presented noise reductions up to 7 dB on a NACA651-210 airfoil at Reynolds number between 2 and $8.3 \cdot 10^5$ at low frequencies and an increase in noise level at high frequencies. Oerlemans et al. [6] analyzed the influence of the trailing-edge serrations on a real wind turbine blade of 94m of rotor diameter and a noise reduction of 3.2 dB was achieved with the use of these devices. However, only recently it has been demonstrated that the practical realization of the serration design alters the flow streamlines at the roots of the teethes, with severe repercussions on the aeroacoustic and aerodynamic performance of the device [7,8]. Although the mechanism behind the noise reductions due to

* Corresponding author.
E-mail address: ellorente@nordex-online.com (E. Llorente).

https://doi.org/10.1016/j.renene.2019.08.128
0960-1481/

the presence of trailing-edge serrations is both experimentally and numerically well documented (e.g. Refs. [9,10]), the aerodynamic influence of these devices on wind turbine performances has not been thoroughly studied. One of the most interesting studies on the aerodynamic performance of these passive treatments is presented by Liu et al. [11]. In their work, a detailed analysis of the aerodynamic performance, wake development and turbulence level of airfoils with trailing-edge serrations has been carried out in order to better understand the noise reduction mechanism. This has motivated a detailed analytic study of the aerodynamic performance change of airfoils with trailing-edge serrations by the authors [12]. In their previous study, a simple prediction law for the changes in lift coefficient of an airfoil with serrations has been proposed downstream of a detailed analysis of the aerodynamic performance of an airfoil with and without add-ons. In this manuscript, the analysis of the change in performance is extended to an already operating wind turbine. The manuscript starts with an experimental analysis of an airfoil with and without serrations, carried out in the low-speed low-turbulence wind tunnel of TU Delft. The aerodynamic performance of two different airfoils extensively used in wind turbine blades with and without trailing-edge serrations are measured under clean and rough conditions. The influence of the flap angle (the angle between the chord of the airfoil and the trailing-edge extensions) has also been measured during the campaign. The experimental data validate the law derived by Llorente et al. [12] for predicting the lift coefficient of an airfoil with trailing-edge serrations from the original lift of the clean airfoil. The manuscript continues by extending the formula to a prediction methodology to evaluate the influence of the serrations on the different airfoils that form a wind turbine blade. With this information, the influence of the trailing-edge serrations on the loads and power production of a real wind turbine can be quantified. The theoretical power production has been compared with the experimental data from Nordex wind turbines with and without trailing-edge serrations operating in the same wind farm.

2. Design and testing of the serrated devices

2.1. Wind tunnel facility

The low-speed low-turbulence wind tunnel of TU Delft was used to first test the serrated edge designed for two wind turbine airfoils. The atmospheric closed-loop wind tunnel has a test section 1.80 m wide, 1.25 m high and 2.60 m long. The 2.9 m diameter six-bladed fan engine, driven by a 525 kW DC motor, delivers the flow through a contraction of 17.8 to the test section at a maximum velocity of 120 m/s. The free-stream turbulence level in the test section varies from 0.02% at 25 m/s to 0.07% at 75 m/s. Electrically actuated turntables flushed with the test-section top and bottom wall provide positioning and attachment of several two-dimensional models, which can be operated at several angles of attack. The centre of rotation for all the models is set at half chord distance. The free-stream velocity is monitored by evaluation of the free-stream dynamic pressure q_0 through a calibration curve from the tunnel contraction control pressure Δp_b, measured as the difference between the settling chamber total-pressure and the wall (static) pressure at a station about half-way in the contraction. The static pressure at the contraction is evaluated as the average of 4 static-pressure taps distributed at the circumference of the tunnel. In this facility, lift and drag are typically measured with a six-degrees of freedom multi-component balance connected to the model. In this particular study, the aerodynamic forces and pressure distribution could be easily obtained from pressure ports distributed on the pressure and suction side of the models (see following section). The pressure tabs features a 13-degrees offset in span-wise direction to avoid mutual pressure orifices interference. The lift coefficient is calculated from the pressure ports using the following Equation (1).

$$C_l = C_n \cos\alpha - C_t \sin\alpha \tag{1}$$

The drag of the airfoil is instead obtained from integration of the measurements from a wake rake of Pitot tubes installed at a distance of half meter downstream the airfoil. The free-stream total-pressure is calculated as an average of all the wake-rake total-pressures outside the wake of the airfoil. Finally the free-stream static-pressure is calculated as the difference between the total pressure from the wake rake and the dynamic pressure from the tunnel controller. Using Equation (2) the drag coefficient could be calculated from the wake-rake information.

$$C_d = 2\int_a^b \left(\sqrt{\frac{q_2}{q_1}} - \frac{q_2}{q_1}\right) \tag{2}$$

In Fig. 1 the layout of the low speed low turbulence wind tunnel is displayed.

2.2. Experimental model and serrations

Two different airfoils have been tested in this first part of the study. The first model is a cambered Nordex ADO30 airfoil with 30% of relative thickness typically used in wind turbine blades (the airfoil profile of the model is protected by non-disclosure agreement). The profile has been manufactured into a straight wing of 600 mm chord and 1225 mm span and installed in the LTT test-section. The wing was manufactured in glass-fiber and resine by the company Streifeneder (https://www.streifeneder.com/) and instrumented with 90 pressure ports, 45 on the suction side and 45 on the pressure side of the airfoil. The second tested model corresponds to a NACA64$_3$418 airfoil, built into an aluminum wing with 250 mm chord and a span of 1225 mm. Due to the relatively smaller chord, a reduced amount of pressure ports (50 pressure, 25 on each side) was used for its instrumentation. Serrations were designed based on the boundary layer information of the different studied airfoils. According to Gruber et al. [10] there is a critical value of $\frac{2h}{\delta} \sim 0.5$ or $\frac{2h}{\lambda} \sim 1$ above which significant noise reductions occur. Increasing this value, noise in low and medium frequencies is reduced but penalties are found at high frequencies. An average between these two values has been selected. The resulting serrations length for the ADO30 airfoil model with the computed boundary layer thickness is $2h = 112$ mm with $\frac{\lambda}{2h} = 0.75$. While for the NACA64$_3$418 model, the resulting trailing-edge serrations geometry is $2h = 75$ mm with $\frac{\lambda}{2h} = 0.75$. Three different flap angles (β) are measured 0°, 5° and 10°. For the second model, the length of the serrations is $2h = 75$ mm with $\frac{\lambda}{2h} = 0.75$. The same three different flap angles have been tested. The trailing-edge serrations for both models have been manufactured in aluminum and have been installed at the pressure side of the models with a 50 mm plate ensuring a smooth transition between the model and the attachment of the trailing-edge extensions. In Fig. 2 and Fig. 3 the reader can find two simple schematics of the serration geometry as well as pictures of both tested models. Boundary layer transition in turbulent conditions is forced by means of a zig-zag tape of 0.4 mm height, and 6 mm length and 6 mm width, placed at 10% of the chord in the pressure side and at 5% of the chord in the suction side. The effectiveness and uniformity of the boundary-layer forcing device was verified by combined use of a remote stethoscope probe and a thermal camera visualization along the wing span.

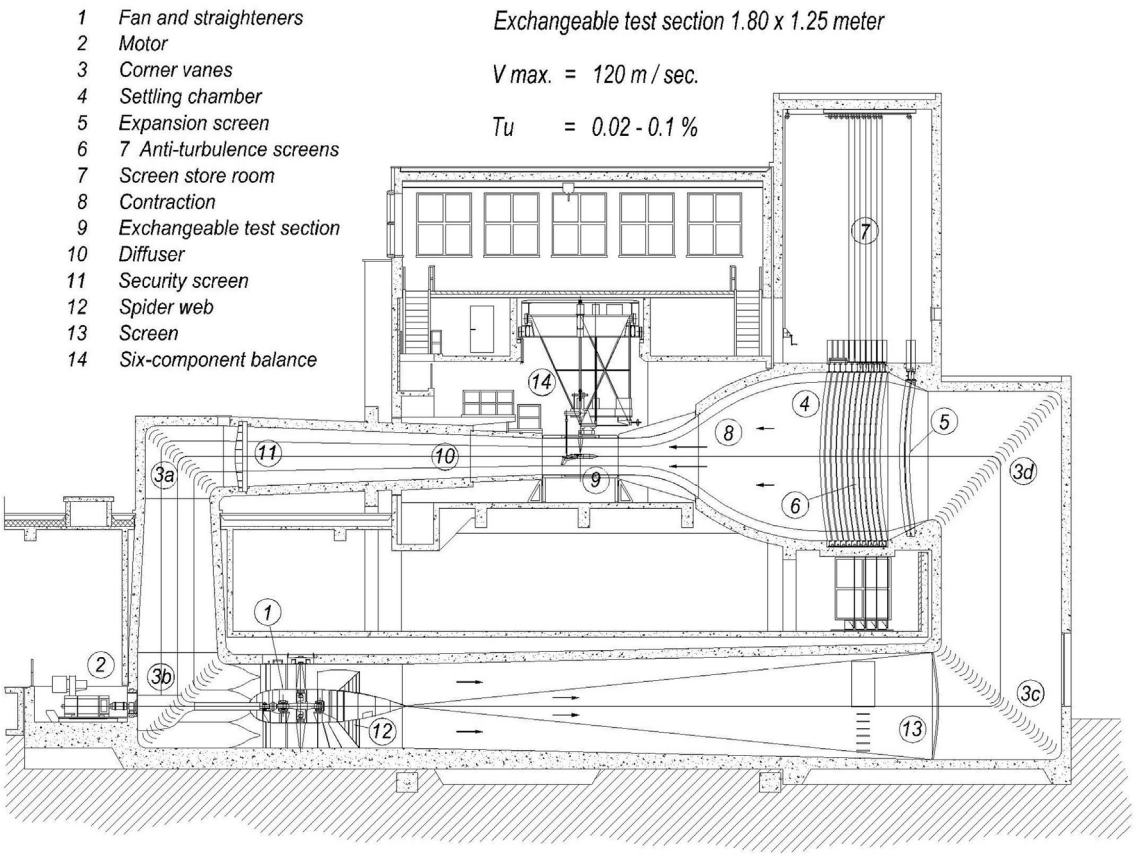

Fig. 1. TU-Delft low speed low turbulence wind tunnel layout.

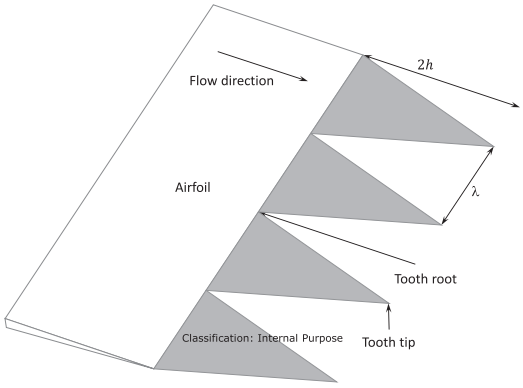

(a) Serrations extensions with length 2h and amplitude of λ

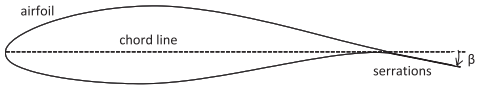

(b) Trailing edge serrations flap angle

Fig. 2. Schematics of the principal parameters of the serrations geometry.

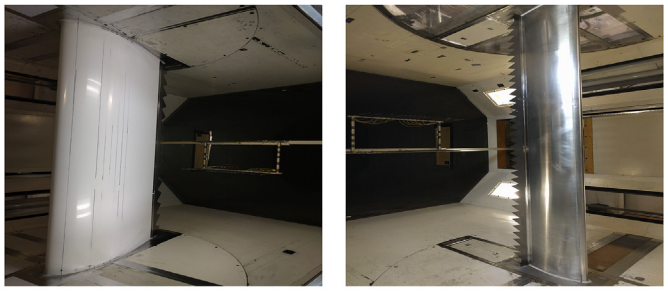

(a) Nordex ADO30 airfoil (b) $NACA64_3418$ airfoil

Fig. 3. Two different airfoil models tested with and without trailing-edge serrations.

3. Wind tunnel results

The aerodynamic results from the wind tunnel tests are used for the prediction of the changes in performance due to serration installation which will be used in the full wind turbine study. Aerodynamic forces have been measured for both the $NACA64_3418$ and the ADO30 with and without trailing-edge serrations in an angle of attack range between −20 and 20°. The wind tunnel is operated at a speed of 75 m/s, respectively corresponding to a chord-based Reynolds number of $Re_c = 1 \cdot 10^6$ for the $NACA64_3418$ and of $Re_c = 3 \cdot 10^6$ for the ADO30. The designed serrations are tested in the range of flap angles: $\beta = 0°, 5°, 10°$. As already mentioned, measurements with free and force boundary-layer conditions have been conducted.

3.1. Nordex ADO30 results

The aerodynamic coefficients for the clean configuration of the ADO30 airfoil at $Re_c = 3 \cdot 10^6$ have been measured and presented in Fig. 4 for different serration flap angles. From analysis of the lift curves, the trailing-edge serrations are found to behave as a flap of a reduced serration length [12], causing a significant increment of lift in the range of investigated angles of attack. A drag increase of about 20% due to the presence of the extensions is appreciated with respect to the baseline configuration. For the baseline airfoil, while the Cl/Cd performance decrease at high serration flap angle (cambering of the airfoil) for angles of attack in the linear Cl range, the max Cl/Cd performance increase instead. This is due to a beneficial camber increase with the flap angle, which increases the max lift produced for the same stall angle of attack. As can be seen in fact from Fig. 4, the stall angle of the airfoil is independent of the presence of the trailing-edge extensions and of the flap angle. This is perhaps due to the loading optimization with which the airfoil profile was obtained.

In the following paragraph, it is interesting to evaluate the effect of boundary-layer forcing with respect to the particular airfoil shape. Boundary-layer forcing is obtained by use of the zig-zag tape as reported in the experimental-setup paragraph. The aerodynamic coefficients measured under forced turbulence conditions are reported in Fig. 5. This configuration shows a considerable difference from the clean case for all tested models. A reduction of 50% on maximum lift coefficient for the non-serrated model is measured with respect to the clean configuration. For the serrated shapes the drop in lift coefficient is still significant but the tendency of lift increase with the flap angle is maintained. At negative angles of attack the flow remains attached and all the curves collapse to similar values. From medium to high angles of attack, between 5° and 20°, the lift coefficient shows a big increase between the serrated and the non-serrated cases. For the serrated models with flap angles of 5° and 10°, similar drag coefficient values are measured and slight increments in lift coefficient were achieved.

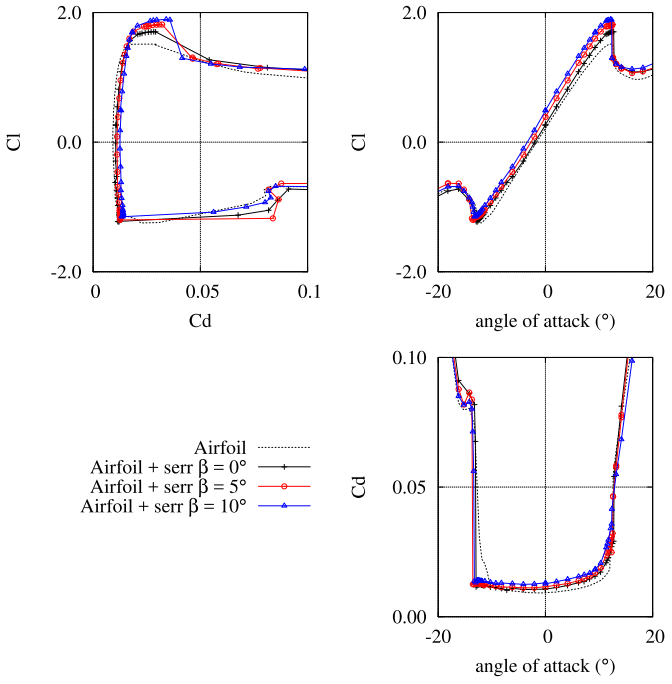

Fig. 4. Aerodynamic coefficients measured for the Nordex ADO30 clean airfoil with and without trailing-edge serrations at different flap angles. Flap convention: positive, pitching towards the pressure side.

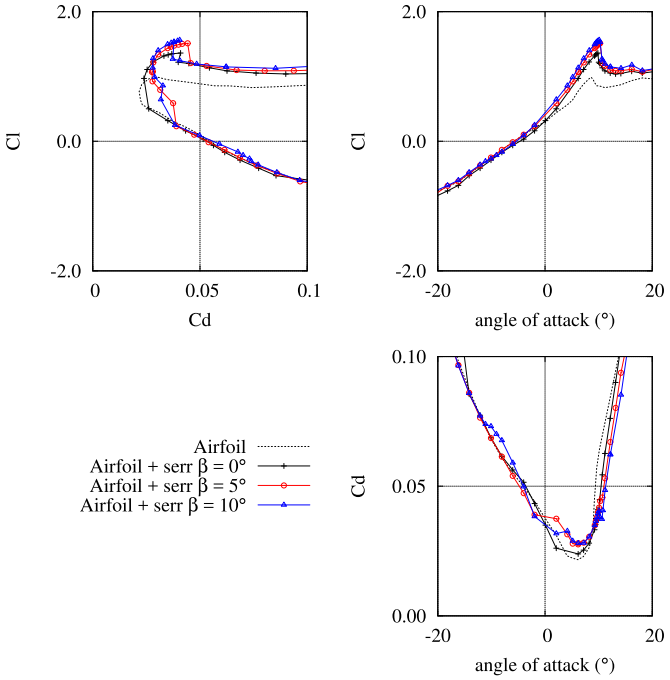

Fig. 5. Aerodynamic coefficients measured for the Nordex ADO30 airfoil under forced boundary-layer transition with and without trailing-edge serrations at different flap angles. Flap convention: positive, pitching towards the pressure side.

These experiments show that the sensitivity of these airfoil to roughness is important and a notable loss of performance is measured for all the cases, with and without trailing-edge serrations.

3.2. NACA64$_3$418 airfoil

The aerodynamic coefficients for this model, measured without and with trailing-edge serrations at different flap angles are presented in Fig. 6. One of the most important aspects for the repeatability of the measurements for this airfoil, is the proper installation of the serrated edges. The relatively lower model chord with respect to the ADO30 requires a careful installation of the serrated devices and a small manufacturing adaptation of the plate for ensuring that 0° flap actually corresponds to the actual camber-line. Important differences between the original airfoil and the serrated configurations are here as well observed. The most significant increments in lift coefficients were achieved in the range of attached flow at angles of attack between 5° and 15°. From analysis of the drag curves, the NACA64$_3$418 seems to have a lower sensitivity to the flap angle change of the serration. Lift and drag coefficients increase indeed with the flap angle, but for this airfoil the increase in Cl/Cd performance is more uniform in the entire angle of attack regime. The serrated trailing-edge with flap angle of 5° seems to be the most effective extension. At angles of attack near the maximum lift the efficiency of the airfoil is again the most significantly amplified by the presence of trailing-edge serrations. Interestingly, the hysteresis loop at positive and negative angles of attack is much more pronounced for this airfoil than for the ADO30. The max difference in lift and drag coefficients when approaching the stall angle of attack from two different sides is of about 60%. This hysteresis is typically consequence of the presence of a laminar separation bubble, which abruptly separates the flow at a specific chord-wise location. The hysteresis cycle is typically not affected by the trailing-edge extension (additionally confirmed in this study),

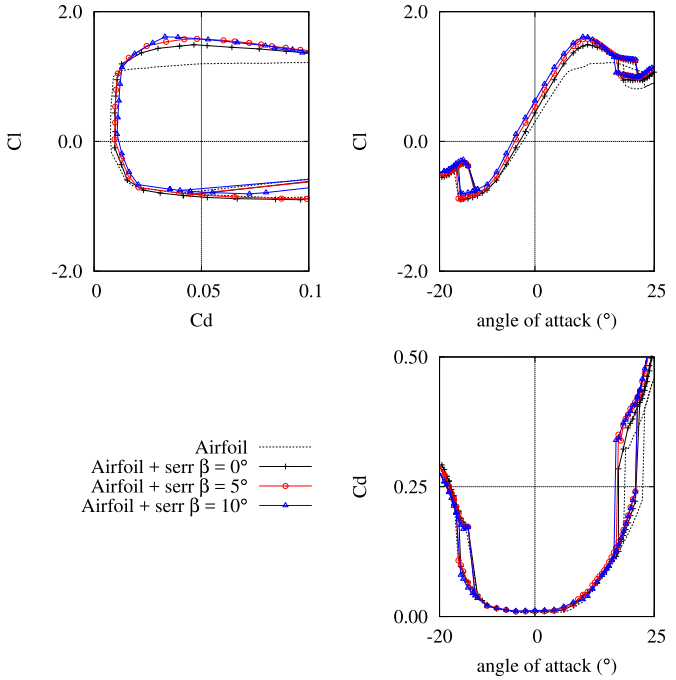

Fig. 6. Aerodynamic coefficients measured for the NACA64$_3$418 clean airfoil with and without trailing-edge serrations at different flap angles. Flap convention: positive, pitching towards the pressure side.

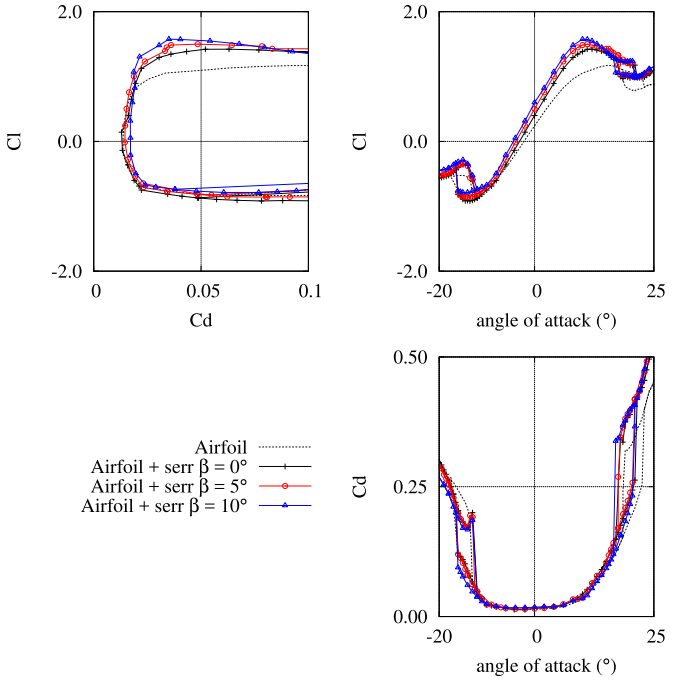

Fig. 7. Aerodynamic coefficients measured for the NACA64$_3$418 under forced boundary-layer transition conditions with and without trailing-edge serrations at different flap angles. Flap convention: positive, pitching towards the pressure side.

due to the sensitivity of the bubble to the peak pressure gradient in proximity of the nose (cfr. Fig. 6). Another peculiar characteristics of this laminar airfoil is the dependence of the stall angle to the airfoil camber. This is a peculiarity of the NACA6-digit airfoils which are based on a particular curvature line which is designed to maintain the flow laminar for most of the airfoil surface [13]. Modification of the camber for this airfoil by extension with a trailing-edge flaps delays therefore the stall angle, but does not substantially change the max lift performance.

In the following, the performances of the NACA64$_3$418 have been evaluated under forced boundary-layer conditions with the use of a zig-zag tape as explained in the experimental-setup section. In Fig. 7 the aerodynamic coefficients are presented for the airfoil with and without trailing-edge serrations. Oppositely to the ADO30, the NACA64$_3$418 is much less sensitive to the boundary-layer transition location. The maximum differences in lift coefficient for the baseline airfoil under free and forced boundary layer conditions are within 15%. Also the effect of the trailing-edge serrations is, therefore, remarkably similar to the clean case. A significant increase in lift coefficient is achieved for the investigated flap angles, this time without affecting the drag coefficient. This is a peculiarity of the particular airfoil which favours attached flow for most of the surface extension. The effectiveness of the airfoil with serrated extensions is much more pronounced for positive angles of attack than for negative ones. In the stall region, as in the clean configuration, the presence of serrated extensions increases the stall angle of attack and the hysteresis loop. The increase in the flap angle does not affect the airfoil hysteresis.

4. Trailing-edge serrations aerodynamic modelling and validation

In this section the measurements performed in the LTT wind tunnel have been used for validating the prediction-law proposed by the authors [12]. The particular law, once experimentally validated for the changes in lift coefficient for the airfoil, can be used as an analytic input in the load and power performance output estimation of a full wind turbine. The law easily modifies the original airfoil data by considering the serrations main geometric parameters (length and flap angle) and the lift coefficient of the original airfoil at zero angle of attack for predicting the effect on lift coefficient of an airfoil with trailing-edge serrations. The formula can be implemented for different airfoil sections along the wind turbine blade. 3D effects along the span on the change of serration performances can be easily neglected given that: 1) serrations are typically applied at the most outboard region of the blade due to the dependence of the sound produced to the 5–6th power of the relative flow speed on the airfoil section [6]; 2) the serration extension is typically contained within 20% of the airfoil chord to avoid flap angle deflections and for reducing maintenance issues. The formulation of the equation used in this manuscript is the one from the authors [12] and presented in Equation (3):

$$Cl_{as} = 2\pi\alpha(1 + l_s/c) + 2\pi\beta l_s/c + Cl_0 \tag{3}$$

Starting with the ADO30 airfoil model and using the l_s of the tested trailing-edge serrations, the chord of the model, c and Cl_0 information obtained from the experiments of the airfoil without trailing-edge extensions in the previous prediction law (Equation (4)), the lift coefficient for the different tested flap angles can be calculated and compared to the experimental results. In Fig. 8 the predicted and measured lift coefficient for this model with trailing-edge serrations varying its flap angle have been displayed. A relatively good agreement is found between the predicted and measured lift coefficient for this configuration for the indicated flap angle till the stall region. The simple linear model is not taking into account the flow separation region in fact.

In Fig. 9 the comparison is extended to the NACA64$_3$418 geometry with Equation (4). As in the previous case a good agreement between the measured and the predicted lift coefficient is obtained for all the different flap angles.

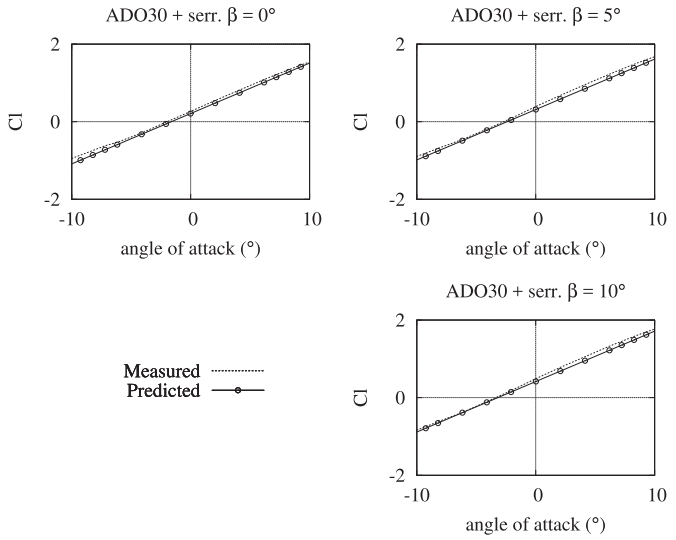

Fig. 8. Comparison between the predicted and measured lift coefficient for the ADO30 airfoil with serrations at varying flap angles.

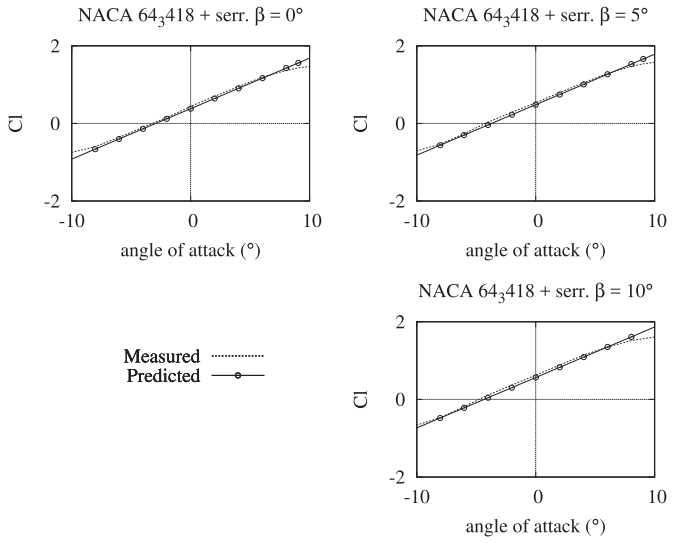

Fig. 9. Comparison between the predicted and measured lift coefficient for the NACA64$_3$418 airfoil with trailing-edge serrations varying the flap angle.

With Equation (4) it has been proven that the lift coefficient of an airfoil with trailing-edge serrations can be predicted from the data of the original airfoil. This equation is also valid for obtaining the lift coefficient under forced boundary-layer conditions although a flap angle correction should be included due to the camber change caused by the forced turbulent conditions. Using this information in the following paragraph a load and power production calculation is performed to evaluate the effect of the serrations in the aerodynamic efficiency of a wind turbine.

5. Trailing-edge serrations effect on the behaviour of a wind turbine

In order to extend the formulation used for the airfoil section to the full blade analysis, the code Bladed [14] has been used. The particular code in the last decades has been extensively used in many industrial standards, since able to provide with an aero-elastic design tool, which still takes into account the machine and its environment. For this study a real wind turbine from Nordex has been simulated. In particular, the AW125/3000 IEC IIIb [15] is a 3 MW machine operating with blades of 61.2 m length and a concrete tower of 120 m. The blades have been designed using similar airfoils than the studied in this manuscript. Serrations have been installed in the last 40% of the blade length, and the polar data of the airfoils have been used in the performance evaluation. Two analysis have been carried out in the following sections: a first evaluation of the serrations influence on the power production of the wind turbine and a study of the serrations impact on the wind turbine loads.

5.1. Wind turbine power production

To analyze the influence of the serrated blade on the power production of the wind turbine a dynamic power curve based on the IEC 61400–12 Ed. 1.0 guidelines [16] has been performed. Several cases for each wind speed from 3.5 m/s to 25 m/s each 0.5 m/s using different wind seeds have been simulated in normal operation. For the original and the serrated cases the same wind turbine control has been used. In Fig. 10 the differences between the electrical power of the original and the serrated rotors for different wind speed are displayed. In this picture increments above 1.5% between serrated and non serrated configurations are obtained, these deviations caused an increase in annual energy production (AEP) around 1% for the serrated configuration.

5.2. Wind turbine loads

To evaluate the influence of the serrations on the loads of the AW125/3000 IEC IIIb wind turbine the IEC 61400–1 Ed. 2.0 guideline [17] has been used. This guideline is the reference standard for wind turbine load calculations and it accounts for several loading typologies, including: aerodynamic forces, weight of the components, inertial forces (e.g centrifugal and gyroscopic forces on the rotor) and additional loading for the wind turbine control system: pitch, torque, yaw and brakes. In this guideline, the procedure for the load evaluation is differentiated between *ultimate* and *fatigue* loading. In the present manuscript a numerical analysis will be carried out on the original design of the AW125/3000 IEC IIIb [15] turbine including the effect of serrations.

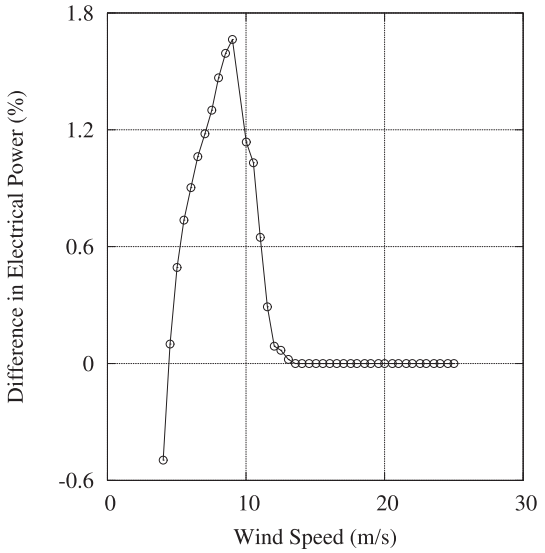

Fig. 10. Difference in electrical power between the serrated and the original wind turbine configuration.

- *Ultimate loads*: this group includes different combinations of loads under operative wind turbine conditions. The resulting loading is derived from the baseline one, once the aero-elastic aspects during design operation of the wind turbine is taken into account. Additional sources as gusts and extreme wind events can be added in conjunction with normal control operations in those geographical locations where necessary. Extra modules of the guidelines allow to treat additional specific control failures, which typically are not intended to simultaneously occur. The complete description of these cases that should be simulated for wind turbine components structural verification are included in the IEC 61400–1 Ed. 2.0 guideline [17].
- *Fatigue loads*: under this field are included different aspects of the cyclic loading which leads to the turbine failure. One of the most known source of cyclic loading is the gravitational 1P imbalance caused by gravity. Wind turbulence is also accounted as a statistical source of random fluctuations on the design loading of the turbine, mainly associated out of rotor-plane loading. The atmospheric boundary layer additionally causes an asymmetric inflow speed with respect to the rotor plane, that is source of a cyclic loading on the blade, which cannot be corrected by yaw control. Furthermore, extra components derived from the upstream effect of the stagnation point on the tower are also considered in this particular category. As for the previous group the IEC 61400–1 Ed. 2.0 guideline [17] gives information on how to model each one of the discussed contributions.

The estimation of the impact of the serrations in the full loading of the wind turbine follows from application of the previous methodology (including both ultimate and fatigue aspects) on the AW125/3000 IEC IIIb [15] machine. These loads, once included the serrations components, could be iteratively used for the optimization of the wind turbine design and for the analysis of the single components such as wind turbine, gear-box, tower, blades, hub in the manufacturing phase. In this manuscript a correction on the wind turbine operation to account for the extra loading due to serration is proposed.

5.2.1. Ultimate loads

As explained in the previous paragraph different combinations of wind conditions and control modes have been calculated for the IEC 61400–1 Ed. 2.0 guideline [17]. For the analysis of this ultimate loads five different groups have been distinguished, blade root, stationary hub, rotating hub, tower base and tower top. Each group is generally used for the design of a specific part of the wind turbine (e.g. the blade root for the hub design, rotating and stationary hub for the rotating components, nacelle and tower base and top for the tower). Fig. 11 shows the wind turbine axis for the different groups (blade root, hub and tower).

For the post-processing of the ultimate loads an statistical analysis of all the simulated cases was done. From this analysis the maximum load (in absolute value) of all the ultimate loads cases is obtained for each group. It is assumed that this maximum load causes the most important damage on each part of the wind turbine. In Table 1 a comparison between the maximum loads for each group obtained with the serrated and the original configuration has been presented.

Analysis of the ultimate loading Table 1 shows that the serrated devices might cause force variations of about 10–15%. The out-of plane rotor momentum (Mz) is the most affected by the presence of the serrations. Focusing on the tower, this effect has been caused by a power production extreme load case. In this design situation, a wind turbine is running and connected to the electric load but the impact of a gust with loss of electrical connection is simulated. When the grid loss is detected the safety system of the machine increases the pitch angle of the blades to reduce the torque carrying the wind turbine to a controlled stop. This situation causes a relatively increase in the My component at the tower base due to the presence of the trailing-edge serrations that amplify the effect of the gust. This aspect is particularly important in the design phase of the wind turbine. For the blade root, the maximum increments are caused by a different load case, a power production plus occurrence of faults in the protection or internal electrical systems. In this case the out-of-plane and the in-plane aerodynamic loads are higher in the serrated case due to the relatively higher lift produced, which determines a relatively higher blade deflection.

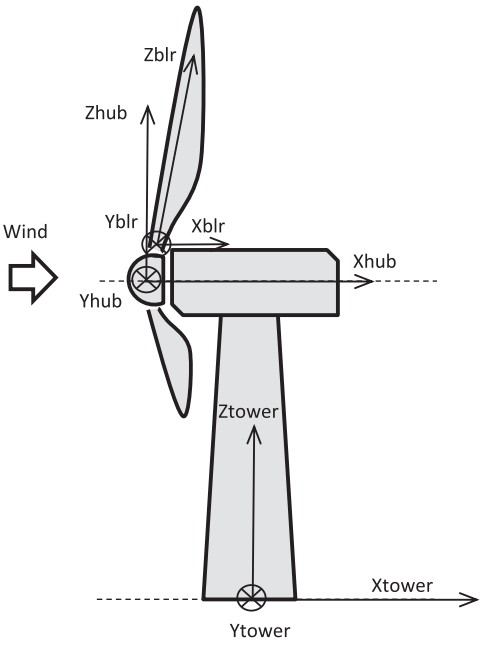

Fig. 11. Wind turbine axis.

Table 1
Ultimate loading comparison: serrated vs. original configurations, positive numbers pertain to an increase in loading with the serrated configuration.

Load	Blade root	Hub fixed	Hub rotating	Tower base	Tower top
Mx	1.38%	0.39%	0.39%	5.91%	1.59%
My	2.07%	3.05%	6.10%	13.95%	2.29%
Mz	15.63%	5.09%	8.32%	5.05%	5.04%
Fx	1.72%	3.31%	3.31%	0.39%	5.36%
Fy	1.31%	7.07%	1.79%	4.38%	14.57%
Fz	1.21%	0.64%	−0.54%	0.02%	0.11%

5.2.2. Fatigue loads

The fatigue loading is assessed by simulating a 10-min operation. The aero-elastic components of the loading is taken into account. The wind turbine model is fed with a turbulent synthetic wind file that accomplishes a frequency spectra. The load signals in different wind turbine locations are accumulated in the fatigue-cycle count. The Rainflow Counting represents a family of methodologies to transform the loading spectrum into fatigue cycles [18]. Besides, a damage equivalent load on the basis of the Palmgren-Miner method [17] is adopted as the range of a sinusoidal load of constant frequency which would produce the same fatigue damage as the original signal. In Table 2 a comparison between the

Table 2
Fatigue loads differences between the serrated and the original configurations.

Load	Blade root	Hub fixed	Hub rotating	Tower base	Tower top
Mx	0.03%	0.99%	0.99%	1.92%	0.78%
My	2.09%	1.28%	1.81%	1.03%	1.81%
Mz	5.34%	2.63%	1.43%	2.20%	2.20%
Fx	1.33%	3.78%	3.78%	2.77%	1.32%
Fy	0.03%	2.92%	0.02%	1.86%	2.86%
Fz	−0.04%	0.02%	0.06%	1.04%	1.04%

serrated and the original wind turbine fatigue loads is shown, as in the previous case, five different load groups have been distinguished, blade root, hub fixed, hub rotating, tower base and tower top.

As in the extreme cases, the fatigue loads are increased due to the presence of trailing-edge serrations. Bigger chords and higher lift coefficients compared to the original configuration have a direct impact on the fatigue loads. The wind turbines are normally design for resisting 20 years of operation, increasing the fatigue loads due to the presence of trailing-edge serrations derive in a component life reduction that should be take into consideration.

6. In-field measurements, validation of the IEC 61400–12 Ed. 1.0 guideline

In this section an analysis of the impact of installing trailing-edge serrations in a real wind turbine has been performed. Two AW125/3000 IEC IIIb wind turbines have been analyzed, one with trailing-edge serrations and another without these devices. Both wind turbines are sited in the same wind farm, in Fig. 12 a photo of the real wind turbines and a shematic of the wind farm layout are displayed. The distance between wind turbines is 1.6 times the rotor diameter and both wind turbines are sited in the same line of the wind farm. The VI-04 wind turbine is the one in which the serrations have been installed (serrated wind turbine) and the VI-06 wind turbine is the machine with the original configuration (control wind turbine) using for control purposes. Both wind turbines have been studied for a period of one year. The VI-04 wind turbine has been operating for 6 months with the same configuration of the VI-06 and after this period the serrations have been installed in the VI-04 wind turbine and another 6 months for both wind turbines have been analyzed. After the serrations installation no changes in the control of the VI-04 wind turbine have been introduced so both wind turbines have been operating with the same controller for the whole period of one year. All the data have been filtered using the valid wind sector (from 60° to 110°).

For the analysis, as no meteorological mast data are available, the wind speed coming from the nacelle anemometer has been used. The power data of the control and the serrated wind turbines have been analyzed distinguishing to different time-lines: before the serrations installation (Timeline 1) and after serrations installation (Timeline 2). For the calculation of the measured power curve the 'method of bins' have been applied [16] using 0.5 m/s bins by calculation of the mean values of the wind speed and power data for each wind speed bin according to the Equation (5):

$$V_i = 1/N_i \sum_{j=1}^{N_i} V_{n,i,j}$$
$$P_i = 1/N_i \sum_{j=1}^{N_i} P_{n,i,j} \quad (4)$$

where V_i is the averaged wind speed in bin i, $V_{n,i,j}$ is the wind speed of data set j in bin i, P_i is the averaged power output in bin i, $P_{n,i,j}$ is the power output of data set j in bin i and N_i is the number of 10 min data sets in bin i. In Fig. 13 the power curves of the control and the serrated wind turbine distinguishing the two different time-lines are depicted. The graph of the control wind turbine shows small

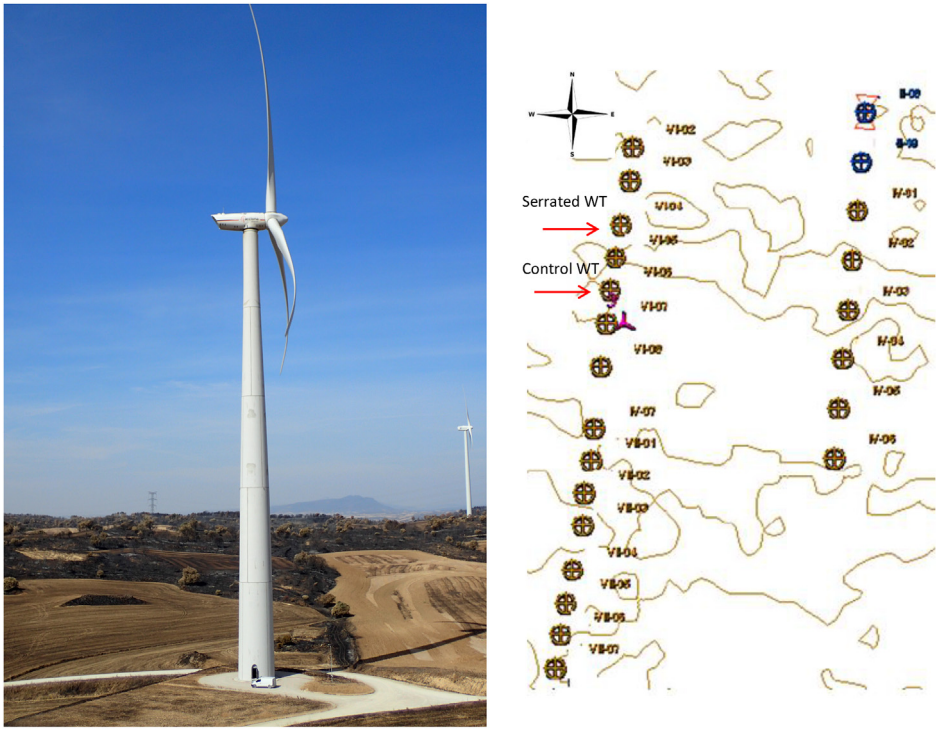

(a) Studied wind turbines (b) Layout of the wind farm

Fig. 12. Studied wind turbines and layout of the wind farm.

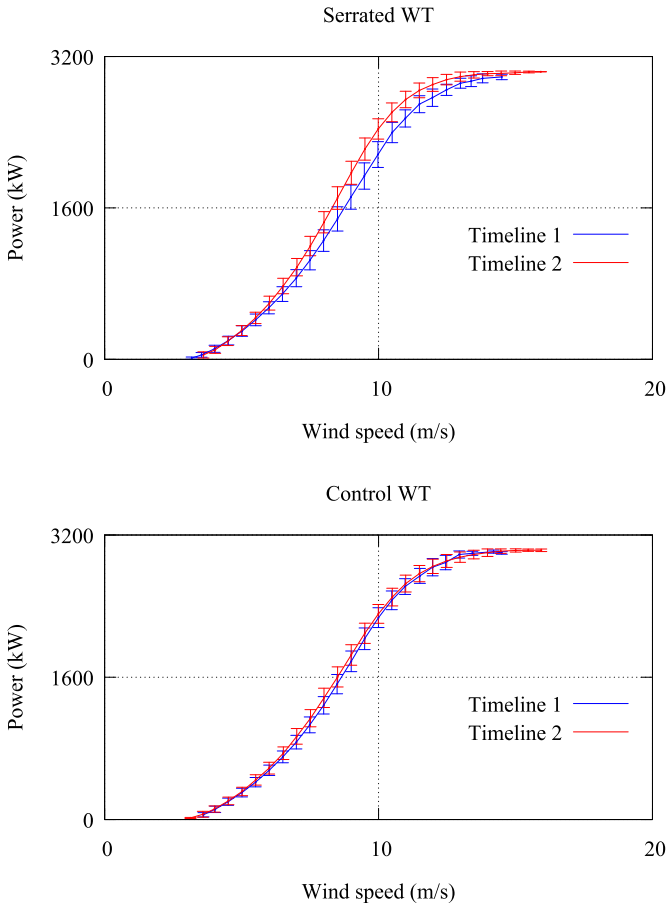

Fig. 13. Power curve for the control and serrated wind turbines before and after the serrations installation.

differences in power curve between both time-lines, these slight differences that show higher power curve for the time-line 2 are due to the change of the environmental conditions of the campaign as now changes in the wind turbine configuration have been made. In the serrated power curve higher differences are observed for the time-line 2 (after serrations installation), part of these changes are due to he environmental conditions, as it is shown for the control wind turbine, but it is clear that the serrations generate an increment in the power curve significantly higher than expected by the theoretical calculations. The annual energy production (AEP) is estimated by applying the measured power curve to different reference wind speed frequency distributions. A Rayleigh distribution, which is identical to a Weibull distribution with a shape factor of 2, has been used [16]. The AEP estimation have been made for a hub height annual average wind speed of 7.6 m/s which is the value of this wind farm. With these conditions, the AEP difference between both time-lines of the serrated wind turbine is around 9% while for the control wind turbine the difference between both time-lines is around 3%. Analyzing the measurement uncertainties it can be obtained that the AEP uncertainties of this power measurements are around 6% for this annual average wind speed, this value agrees with the typical uncertainty for these campaigns documented in different experimental studies [19,20].

7. Conclusions

A complete analysis of the influence of the trailing-edge serrations on a real wind turbine has been performed starting from the airfoil and serration design and testing. An experimental analysis of two different airfoils extensively used in wind turbines (and for the tested turbines AW125/3000 IEC IIIb) has been carried out to analyze the impact of the trailing-edge serrations on the airfoils behaviour. Aerodynamic coefficients of the airfoil with trailing-edge serrations have been compared to the results of the original airfoil in clean and rough conditions. For both airfoils, the lift coefficient is always increased by the presence of these extensions mainly in the maximum lift region. The drag is negligibly increased together with the lift, so the efficiency of the airfoil is overall improved. The stall angle is not influenced by the presence of the devices in any case. Analyzing the influence of the serrations flap angle the lift and drag coefficients increase also in clean and rough conditions. Using the lift prediction law the influence of the serrations can be extended to the rest of the airfoils of a blade and the impact of installing these devices in a real wind turbine has been studied. The loads and the power curve of a wind turbine with trailing-edge serrations have been calculated and compared to the original configuration. An increase on loads and power curve have been obtained due to the presence of these trailing-edge extensions, which is balanced by an increase of the fatigue cycle. The effect of serrations is quantified within 5% in mean loading and within 1% in power variation with respect to the original configuration. The analysis of the experimental data on a real wind turbine shows higher power curve due to the presence of the trailing-edge serrations that consequently give more production than theoretically expected. This significant power increment will cause higher loads on the wind turbine that reduce its lifetime. A more detailed study on real wind turbines focusing on load analysis at different parts of the machine should be done to clarify the impact of the trailing-edge serrations on the loads and lifetime of a real wind turbine.

References

[1] M. Howe, Aerodynamic noise of a serrated trailing edge, J. Fluids Struct. 5 (1991) 33–45, https://doi.org/10.1016/0889-9746(91)80010-B.
[2] M.S. Howe, A review of the theory of trailing edge noise, J. Sound Vib. 61 (3) (1978) 437–465, https://doi.org/10.1016/0022-460X(78)90391-7. URL, https://doi.org/10.1016/0022-460X(78)90391-7.
[3] L. Jones, R. Sandberg, Direct numerical simulations of noise generated by the flow over an airfoil with trailing edge serrations, in: Aeroacoustics Conferences, American Institute of Aeronautics and Astronautics, 2009, https://doi.org/10.2514/6.2009-3195. URL, https://doi.org/10.2514/6.2009-3195.
[4] L.A.B.D.J. Moreau, M.R. Tetlow, C.J. Doolan, Acoustic analysis of flat plate trailing edge noise, in: I.C.A. (Ed.), Proceedings of 20th International Congress on Acoustics, ICA, 2010.
[5] M.A. Mathieu Gruber, P.F. Joseph, Airfoil trailing edge noise reduction by the introduction of sawtooth and slitted trailing edge geometries, in: Proceedings of 20th International Congress on Acoustics, ICA, 2010.
[6] S. Oerlemans, M. Fisher, T. Maeder, K. Kögler, Reduction of wind turbine noise using optimized airfoils and trailing-edge serrations, AIAA J. 47 (6) (2009) 1470–1481, https://doi.org/10.2514/1.38888. URL, http://arc.aiaa.org/doi/abs/10.2514/1.38888.
[7] F. Avallone, C.A. Leon, S. Pröbsting, K.P. Lynch, D. Ragni, Tomographic-PIV investigation of the flow over serrated trailing-edges, in: 54th AIAA Aerospace Sciences Meeting, American Institute of Aeronautics and Astronautics (AIAA), 2016, https://doi.org/10.2514/6.2016-1012.
[8] D. Ragni, F. Avallone, W.C.P. van der Velden, D. Casalino, Measurements of near-wall pressure fluctuations for trailing-edge serrations and slits, Exp. Fluid 60 (1) (2018) 6, https://doi.org/10.1007/s00348-018-2654-5. URL, https://doi.org/10.1007/s00348-018-2654-5.
[9] C. Arce, D. Ragni, S. Pröbsting, F. Scarano, J. Madsen, Flow topology and acoustic emissions of trailing edge serrations at incidence, Exp. Fluid 57 (5). doi:10.1007/s00348-016-2181-1.
[10] M. Gruber, P. Joseph, T. Chong, On the mechanisms of serrated airfoil trailing edge noise reduction, in: Aeroacoustics Conferences, American Institute of Aeronautics and Astronautics, 2011, https://doi.org/10.2514/6.2011-2781. URL, https://doi.org/10.2514/6.2011-2781.
[11] A.M. Liu X, H. Kamliya Jawahar, R. Theunissen, Wake development of airfoils with serrated trailing edges, in: 22nd AIAA/CEAS Aeroacoustics Conference, American Institute of Aeronautics and Astronautics (AIAA), 2016, https://doi.org/10.2514/6.2016-2817.
[12] E. Llorente, D. Ragni, Trailing edge serrations effects on the aerodynamic

performance of a naca 643418, Wind Energydoi, https://doi.org/10.1002/we.2293.
[13] I.H. Abbott, A.E. von Doenhoff, Theory of Wing Sections, DOVER PUBLICATIONS, INC., 1959.
[14] DNV-GL, Bladed Technical Brochure, DNV-GL, Bristol, BS2 0PS United Kingdom, June 2015. URL, https://www.dnvgl.com/energy/generation/software/bladed.
[15] AW3000 Brochure, Hamburg, Germany, October 2017. URL, http://www.nordex-online.com/en/produkte-service/wind-turbines/aw1253000.html.
[16] IEC 61400-12 ed.1.0 Guidelines, December 2005.
[17] IEC 61400-1 ed.2.0 Guidelines, August 2005.
[18] V. Passipoularidis, T. Philippidis, P. Brondsted, Fatigue life prediction in composites using progressive damage modelling under block and spectrum loading, Int. J. Fatigue 33 (2) (2011) 132–144. https://doi.org/10.1016/j.ijfatigue.2010.07.011.
[19] K. Franke, A. Albers, Power curve uncertainty of rotor equivalent winde speed, in: Wind Europe conferences, 2016.
[20] German Wind Energy Insitute GmbH (DEWI), Uncertainty of annual energy production for a specific turbine model based on a ser of IEC 61400-12 measurements, URL, https://www.dewi.de/dewi/fileadmin/pdf/publications/Publikations/.